Received: 3 January 2023 | Revised: 19 March 2023 | Accepted: 20 March 2023

DOI: 10.1002/pen.26312

RESEARCH ARTICLE

POLYMER ENGINEERING AND SCIENCE WILEY

Shape memory behavior of novel Ethylene Propylene Diene Monomer (EPDM)/paraffin foams

M. Bianchi | **G. Fredi** | **F. Valentini** | **A. Dorigato** | **A. Pegoretti**

Department of Industrial Engineering and INSTM Unit, University of Trento, Via Sommarive 9, 38123 Trento, Italy

Correspondence
M. Bianchi, University of Trento Department of Industrial Engineering and INSTM Unit Via Sommarive 9, 38123 Trento, Italy.
Email: marica.bianchi@unitn.it

Abstract

Ethylene Propylene Diene Monomer (EPDM) rubber foams are widely employed for thermal and acoustic insulation in building construction. However, their installation in confined spaces is often complicated, and the capability of EPDM foams to exhibit shape memory behavior could be a desirable property. In the literature, several works have demonstrated that blending elastomeric matrices with paraffin, a well-known Phase Change Material (PCM), could be an interesting method to obtain shape memory polymers with a tunable switching temperature. In this work, EPDM foams filled with paraffin wax, having a melting temperature of 70°C, were produced and characterized from a microstructural and thermo-mechanical point of view. By melt compounding and hot pressing, samples were produced, and the PCM content in the foams was varied between 0 and 60 wt% (with respect to the EPDM matrix). The results of the shape memory tests evidenced the crucial role played by the PCM in providing excellent shape fixability for the expanded rubber. Even a limited amount of paraffin (i.e., 20 wt%) was able to raise the strain fixity parameter to a value higher than 80%, and it reached 100% when the paraffin content was increased to 60 wt %. On the other hand, an increased PCM fraction caused a slower recovery process. Consequently, a compromise between a fast recovery and optimum shape fixability should be accepted. These results are promising for the development of novel thermal and acoustic EPDM insulating foams easier to be installed.

KEYWORDS

EPDM, paraffin, polymer foams, rubber, shape memory polymers

1 | INTRODUCTION

Shape memory polymers (SMPs) are smart materials that have drawn much interest due to their practical functions and potential uses in a multitude of sectors, including aeronautical engineering, smart biomedical devices, packaging, and textile engineering.[1–3] The peculiar characteristic of this emerging class of polymers is the capability of storing and recovering large deformations.[4] More specifically, SMPs can fix a temporary shape under specific conditions of temperature and stress and then recover the pristine permanent shape when exposed to appropriate external stimuli, generally involving heating.[5,6]

Shape memory behavior is not an intrinsic property of a given polymer but is the result of a proper polymer structure and thermo-mechanical history.[5,6] SMPs are usually flexible polymer networks that consist of stimuli-sensitive molecular switches and net points. The permanent shape of the polymer is determined by the net points, which may be chemical or physical in nature. The

switching segments are responsible for the fixability of the temporary shape and are characterized by a transition temperature, T_{trans} that acts as a molecular switch. T_{trans} can be a glass transition or a melting temperature.[7,8] The macromolecules exhibit high mobility when the material is heated above T_{trans}, allowing the polymer to be easily deformed into the appropriate temporary shape. Cooling the material under load below T_{trans} strongly reduces its mobility, thereby fixing the imposed deformation. Finally, when the polymer is heated above T_{trans}, the switching domains progressively regain their mobility, and the material returns to its original condition.[8]

Taking inspiration from the structure shown by the most common SMPs, a recent field of research has been focused on finding methods to confer and tune the shape memory behavior of other polymer systems. This aim is of great interest since numerous applications where the polymer's capability to change shape with a proper external stimulus would be desirable, but the structural and thermal characteristics of the material do not allow such behavior.

One possible way to obtain this result is polymer blending.[7–10] For example, it has been recently observed that blending elastomers with organic phase change materials (PCMs), such as poly(ethylene glycol)s, fatty acids, paraffin waxes, etc., is a potential method to ensure optimal shape memory properties to the polymers.[11–14] Organic PCMs have been extensively explored for thermal energy storage (TES) and thermal management applications because of their capacity to store and release a significant quantity of latent heat in a restricted temperature range.[15–31] However, the possibility to confer shape memory behavior to these PCM-containing polymers has only recently come to the attention of the scientific community.[31–33] The solid–liquid phase transition of the PCMs provides the elastomers with the switching phase, and hence T_{trans}, which otherwise would be missing in the original elastomer in the interested temperature interval. In addition, since PCMs are available with a wide range of melting points, it is possible to select the most suitable one depending on the application. The working mechanism of elastomer/PCM shape memory blends can be explained as follows. While the phase transition of the PCM allows fixing the temporary shape imposed on the material, the elastomeric matrix provides the retractive forces to recover the original permanent shape. More specifically, when the polymer blend is heated above T_{trans}, the initial solid PCM becomes liquid and the material can be deformed to a temporary shape. Once the polymer blend is cooled under load below T_{trans}, the PCM crystallizes and blocks the polymer chains of the matrix in their low entropy state configuration, fixing the deformation imposed. Upon re-heating the polymer blend above T_{trans}, the PCM melting causes the removal of such a constraint and the "frozen" retractive forces in the elastomeric matrix promote the recovery to the initial geometry.

In the literature, recent works can be found on elastomeric matrices blended with PCMs showing shape memory properties. For example, the effective role of the PCMs in improving the shape memory behavior of elastomers has been demonstrated by Weiss and colleagues in zinc-neutralized sulfonated EPDM and fatty acids salts,[11] Lu and Yu in EPDM paraffin wax blends,[11] both Sun and Ding in silicone paraffin wax blends[12,13] and Lai and others in natural rubber/paraffin wax/CNT composites.[14] However, only a few of the published works focus on elastomeric foamed matrices.

Elastomeric foams, also known as expanded rubber, are elastomer-and-gas mixtures that have good fire performance, great flexibility, resistance to abrasion and deformation, and low thermal conductivity values.[34–36] These characteristics have made these cellular polymers key materials in our daily life, especially for thermal and acoustic insulation applications.[34,35] The conventional foaming process for expanded rubber production typically involves adding a blowing agent to the elastomers, which as the temperature rises, creates the gases that cause the polymer to expand. As a result, during processing, gas bubbles are created in the viscous polymer matrix, which persists after cooling and creates a cellular structure.[34,37] The blowing agents can be subdivided into chemical and physical blowing agents. The first type is constituted of solid organic or inorganic chemicals that degrade thermally and release gases, while the second type is made up of fluids that evaporate and release gases to allow for polymer expansion.[34,38]

The preparation of rubber foams has been the subject of numerous studies.[34,35] Particularly, among expanded rubbers, EPDM foams have attracted a lot of attention for outdoor applications such as automotive sealing systems, wire materials, building profiles, white sidewalls of tires, electric-electronic components, roofing sheets, and sporting goods due to their peculiar properties.[34–37,39] More specifically, EPDM foams boast numerous advantages, including great resistance to oxidation, ozone, and weathering as well as high chemical stability, impact, and abrasion resistance. However, their installation in confined spaces is often complicated. For example, the installation of tubular foams for the thermal insulation of pipes can be sometimes difficult, since the foam should perfectly adhere and press on the pipe surface. Hence, the capability of EPDM foams to exhibit a shape memory behavior could be desirable to overcome such limitations.

In our previous work,[34] the thermal, mechanical, and TES properties of EPDM foams filled with paraffin (melting temperature 70°C) were investigated, demonstrating that expanded rubbers produced through

TABLE 1 Composition of the EPDM compound.

Material	Quantity (phr)
Vistalon® 2504	100.00
Carbon black (reinforcing filler)	20.00
Stearic acid (activator)	1.00
Zinc oxide (activator)	3.00
Sulfur (vulcanizing agent)	3.00
TMTD[a] (accelerator)	0.87
ZDBC[b] (accelerator)	2.50

[a]TMTD = tetramethylthiuram disulfide.
[b]ZDBC = zinc dibutyldithiocarbamate.

conventional foaming techniques show an interesting potential for thermo-insulating and thermal management applications. For example, they could be applied for the thermal management of electronic devices or pipe systems carrying fluids at temperatures close to 70°C and suffering from thermal fluctuations. In this work, the capability of the PCM to confer shape memory properties to the same EPDM/paraffin foams was explored, in view of easing their installation and widening their applications. To the best of the authors' knowledge, this is the first study to investigate the shape memory performance of EPDM/paraffin foams.

2 | EXPERIMENTAL PART

2.1 | Materials

All the materials used for the foams' production were the same as described in our previous work.[34] To summarize briefly, Exxon Mobil (Irving, TX) supplied the Vistalon® 2504 EPDM rubber. Vistalon® 2504 is an amorphous terpolymer with a broad molecular weight distribution and a Mooney viscosity (ML 1 + 4, 125°C) of 25 MU. It contains 58 wt% of ethylene and 4.7 wt% of ethylidene norbornene. Chemicals used in the vulcanization process included sulfur, zinc oxide, and stearic acid and were provided by Rhein Chemie (Cologne, Germany). As a reinforcing filler, Carbon Black N550 from Omsk Carbon Group (Ontario, Canada) was employed. During the compounding process, tetramethylthiuram disulfide (TMTD) and zinc dibutyl dithiocarbamate (ZDBC), which were acquired from Vibiplast srl in Castano Primo (MI), Italy, was added. The composition of the EPDM compound used for the preparation of the samples is given in Table 1.

For the expansion of EPDM rubber, Hostatron® P0168 (H), supplied from Clariant GmbH (Ahrensburg, Germany), and Micropearl® F82 (MP), acquired from Lehvoss Italia S.r.l. (Saronno, Italy), were used. The physical blowing agent Micropearl® F82 is made up of 20 to 30 μm-diameter microspheres that contain iso-pentane, which expands when the temperature rises over 115 to 120°C due to the evaporation of the hydrocarbon. The chemical blowing agent Hostatron® P0168 is made up of a combination of sodium, calcium, and potassium bicarbonates. At 150°C, the bicarbonates decompose, causing the evolution of carbonates, CO_2, and vapor as reaction byproducts. This causes the expansion.

Rubitherm GmbH supplied Rubitherm® RT70, a paraffin wax with a melting point of 70°C and a melting enthalpy of 260 J/g (Berlin, Germany). Paraffin having a melting temperature of 70°C was selected to provide EPDM foams (used for thermal insulation of pipes) with two combined benefits. The first deals with the thermal management of pipe systems in the event of undesired thermal fluctuation (exploring the thermal energy storage capabilities of the PCM). The second, on the other hand, concerns the possible and desirable installation improvement of the insulating foams by exploring the shape memory behavior conferred by the addition of paraffin to the expanded rubbers, since the PCM could be able to provide EPDM rubber with the switching phase necessary to fix the temporary shape.

2.2 | Sample preparation

Two different kinds of EPDM foams have been prepared and characterized. H was used to produce the first series of foams, while MP was adopted to produce a second series of expanded rubbers. Additionally, the neat foam (constituted only by EPDM compound) and EPDM foams containing 20, 40, and 60 wt% of paraffin (relative to the EPDM compound) were prepared for each series of cellular rubbers. A sample of bulk EPDM rubber was also produced to compare the properties of foamed and unfoamed samples. The procedure followed for the preparation of EPDM and EPDM/paraffin foams (schematized in Figure 1) was the same as reported in our previous work,[34] to which the reader is referred for further details.

The composition of the prepared foams along with their codes is reported in Table 2. The EPDM rubber that is not foamed is the sample with the name EPDM. The term EPDM, the letters that indicate the production process (H for Hostatron foaming agent, MP for Micropearl foaming agent), the letter P, which stands for paraffin (in foams containing the PCM), and then a number that represents the weight % of paraffin in the sample make up the samples' code.

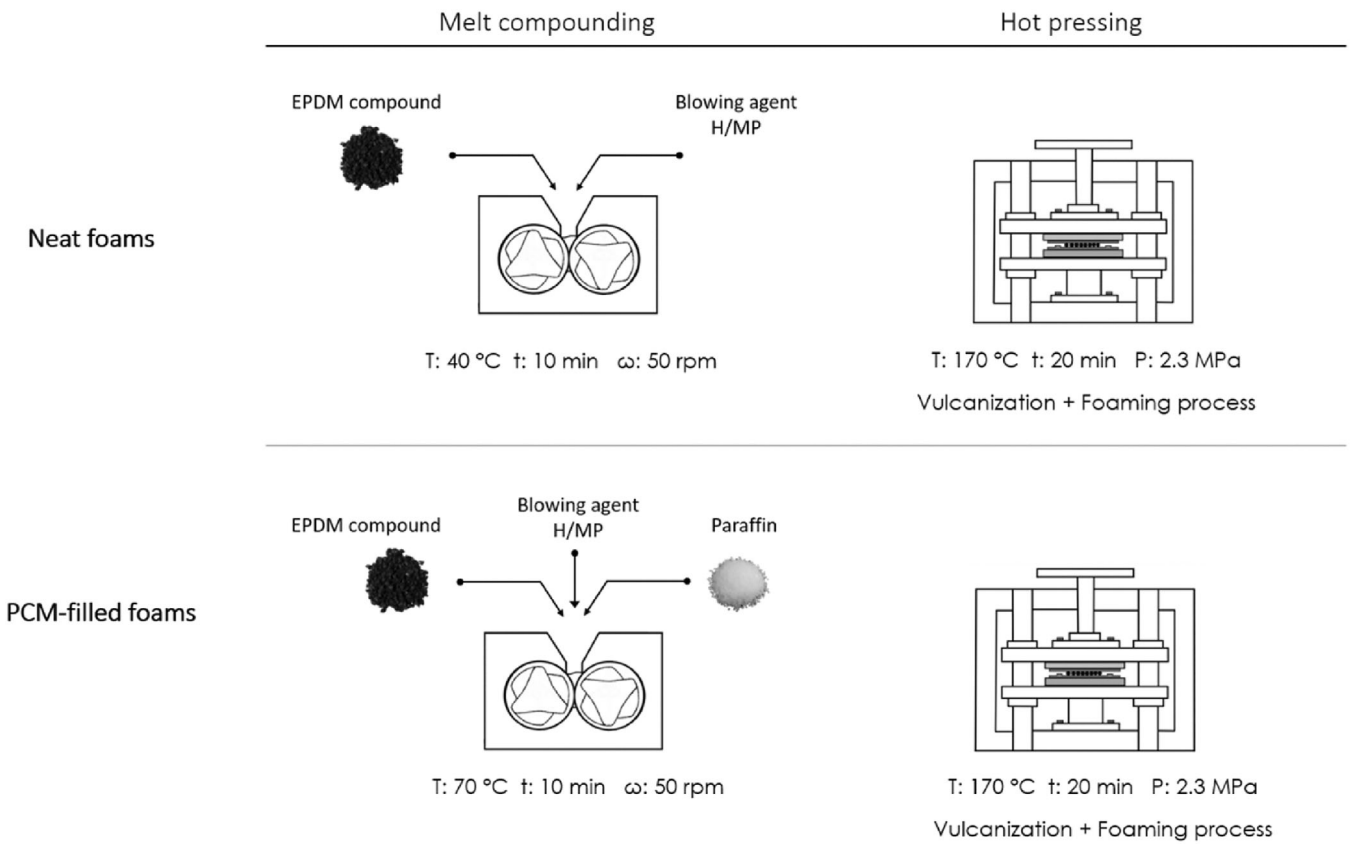

FIGURE 1 Scheme of the production process of EPDM and EPDM/paraffin foams. T: temperature, t: time, ω: rotor speed, P: pressure.

TABLE 2 Prepared samples and their nominal composition.

Sample	Vistalon 2504 (phr)	RT70HC (phr/wt%/vv%)	Micropearl F82 (phr)	Hostatron P0168 (phr)
EPDM	100.0	–	–	–
EPDM_H	100.0	–	–	1.3
EPDM_H_P20	100.0	33.0/20.0/22.0	–	1.3
EPDM_H_P40	100.0	87.0/40.0/43.0	–	1.3
EPDM_H_P60	100.0	196.0/60.0/63.0	–	1.3
EPDM_MP	100.0	–	14.0	–
EPDM_MP_P20	100.0	33.0/20.0/22.0	14.0	–
EPDM_MP_P40	100.0	87.0/40.0/43.0	14.0	–
EPDM_MP_P60	100.0	196.0/60.0/63.0	14.0	–

2.3 | Experimental methodologies

A field emission scanning electron microscope (FESEM) AG-SUPRA 40 (Carl Zeiss, Germany) was used to acquire SEM micrographs of the produced foams' cryofracture surfaces following Pt/Pd sputtering. The acceleration voltage was set at 2.5 kV. ImageJ® software was used to determine the pore diameter of the produced foams and, for each type of cellular rubber, 15 pores were measured. The primary axis of the ellipse was taken into account for cells that had an elliptical form.

Helium pycnometry was employed to determine the apparent densities (ρ_{app}) of the produced EPDM and EPDM/paraffin foams. At a temperature of 23.0°C in helium, tests were performed on specimens weighing approximately 0.2 g using a gas displacement AccuPycII 1330 pycnometer (Micrometrics Instrument Corporation, USA). For each sample, 60 replicate measurements were

performed. Ten square specimens, derived from each EPDM sample, were used to evaluate the geometrical density (ρ_{geom}). The dimensions of the specimens were measured by means of a caliper (sensitivity 0.01 mm) while the mass was determined using a Gibertini E42 balance (sensitivity 10^{-4} g). By dividing the mass by the whole volume, which includes bulk material and both closed and open porosity, ρ_{geom} was determined. According to the ASTM D6226 standard, the fraction of open porosity (OP), the total porosity (P_{tot}), and the close porosity (CP) were determined according to Equations (1–3), respectively.

$$OP = \left(1 - \frac{\rho_{geom}}{\rho_{app}}\right) \cdot 100 \tag{1}$$

$$P_{tot} = \left(1 - \frac{\rho_{geom}}{\rho_{bulk}}\right) \cdot 100 \tag{2}$$

$$CP = P_{tot} - OP \tag{3}$$

where ρ_{bulk} is the material's density without porosity, which in our prior work was reported to be 1.042 g/cm^3 for the unfoamed EPDM sample.[30]

Dynamic-mechanical thermal analysis (DMA) was conducted using a DMA Q800 apparatus by TA Instruments to examine the temperature dependency of the storage modulus, loss modulus, and loss factor of the produced foams. Tests were performed on rectangular specimens (gauge length 10 mm, width 5 mm, thickness 2 mm) in single frequency strain mode at 1 Hz, with strain amplitude of 0.05%, and at a heating rate of 10°C/min in the temperature range from 0 to 120°C. One specimen was tested for each composition. From the results, the storage modulus at 25 and 90°C was determined.

Compression set (CS) measurements were carried out following ASTM D395-85 standard for 22 h at 25 and 90°C. After 30 min at room temperature, recovery measurements were taken. Cylindrical disks, obtained from the produced square foams, were used as test specimens. Depending on the thickness of the foams, dimensions were selected to maintain a constant aspect ratio as dictated by the standard. In more detail, the bulk EPDM specimens and foams made with H foaming agent had a diameter of 14 mm and a thickness of 5 mm, whereas foams made with MP foaming agent had a diameter of 30 mm and a thickness of 10 mm. To maintain the constant deflection defined by the standard, the spacing bar used had, for the former, a thickness of 4.19 mm while for the latter 7.49 mm. Three specimens for each composition and temperature were tested. The CS has been evaluated according to Equation (4):

$$\mathrm{CS}\,(\%) = \frac{t_0 - t_i}{t_{0-t_u}} \cdot 100 \tag{4}$$

where t_0 is the initial thickness of the specimen, t_i the final thickness, and t_u the thickness of the spacing bar. From Equation (4), a CS value of 100% means that the test specimen remains completely compressed and does not return to its original state. On the other hand, if the test specimen returns to its original state a CS value of 0% is obtained.

The shape memory response of the produced EPDM/paraffin foams was investigated following a two-step analysis. First, a preliminary study of the shape memory behavior of the samples was carried out to verify the effective role of paraffin in improving the shape memory performance of neat EPDM foams. After that, a quantitative analysis of the shape memory behavior was performed. In the preliminary analysis, the shape memory behavior was investigated and evaluated on rectangular specimens (length 100 mm, width 10 mm, thickness 5 mm) through a qualitative bend-recovery measurement. The tests were conducted using the standard thermo-mechanical cycle for SMPs, which consists of a programming phase and a recovery step. More specifically, the specimens were subjected to the following thermo-mechanical history: (I) heating of the specimens at 90°C by using an oven, (II) temperature maintenance for 30 min to promote a complete melting of paraffin, (III) bending of the specimens at 90° (IV) cooling down to room temperature under a constant external force, (V) temperature maintenance for 2 h to allow paraffin solidification, (VI) re-heating at 90°C to promote shape recovery. The shape memory recovery behavior was recorded by a digital camera.

The strain fixity (SF) and strain recovery (SR) parameters were used to quantify the shape memory behavior. The first parameter measures the capability of the material of fixing the mechanical deformation imposed during the programming process, while the second one provides information about the extent of strain recovery during the recovery step. In a well-performing SMP, both SF and SR should be close to 100%. For each test specimen, the strain fixity (SF_0) and strain recovery (SR) were calculated using Equations (5) and (6), respectively:

$$SF_0(\%) = \frac{90 - \alpha}{90} . 100 \tag{5}$$

$$SR\,(\%) = \frac{\beta}{90} . 100 \tag{6}$$

where α is the angle presented by the specimen after the shape is fixed and β is the angle presented by the

FIGURE 2 Graphical representation of α and β angle utilized for the determination of the strain fixity (SF) and the strain recovery (SR) parameters.

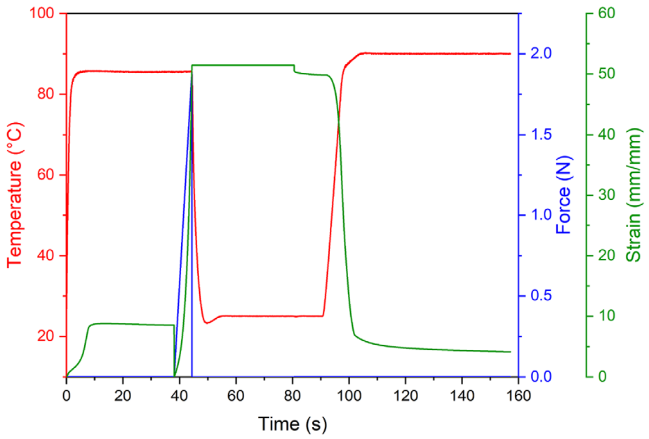

FIGURE 3 Example of the thermo-mechanical cycle adopted for the characterization of the shape memory behavior of the prepared foams.

specimen during the shape-recovery process, as represented in Figure 2. ImageJ® software was used to measure these angles from digital images. In particular, strain recovery was evaluated at six different times after the foams were placed in the oven at 90°C: 0, 100, 200, 500, 1100, and 3600 s. The subscript 0 in Equation (5) indicates that strain fixity was determined immediately after removing the constraint. Moreover, five digital images, for each type of foam taken in the oven at 0 s and when each of the single specimens reaches a complete recovery of the permanent shape, have been reported.

Using the previously described DMA equipment, a quantitative analysis of the produced foams' shape memory behavior was carried out on rectangular specimens with gauge lengths of 10 mm, widths of 5 mm, and thicknesses of 2 mm. The tests were carried out according to a thermo-mechanical cycle similar to the one adopted in the qualitative analyses, and a graphical representation of the cycle is presented in Figure 3. In particular, the specimens were subjected to the following thermo-mechanical history: (I) heating of the specimen and equilibration at 90°C, (II) isothermal hold for 30 min at 90°C, (III) measurement of the length of the specimen, (IV) application of a ramp force of 0.3 N/min, (V) drive-off of the motor when a certain strain ε_{def} is achieved, (VI) cooling and equilibrium of the sample at 25°C, (VII) isothermal for 30 min, (VIII) drive-on of the motor, (IX) application of a constant load equal to 0.001 N to the specimen in order to maintain proper contact and to monitor continuously the sample displacement as a function of the temperature, (X) isothermal for 10 min at 25°C, (XI) heating ramp of 10°C/min to 90°C, (XII) isothermal for 60 min at 90°C.

In step III, the specimen length was measured in order to deform the sample considering as initial length the one after the thermal expansion of the material to avoid an underestimation of the specimen's capability to fix the temporary shape, caused by the recovery of the thermal expansion at step IX.

The deformation imposed at step V was chosen by analyzing the tensile stress–strain curves of the samples at 90°C (reported in our previous work[34]). In particular, a deformation ε_{def} equal to 15% for all neat foams and 50% for paraffin-filled foams was selected, respectively.

To quantify the shape memory behavior, strain fixity, and strain recovery were calculated. Strain fixity at load removal, SF_0, and 600 s after load removal, SF_{600}, was determined according to Equations (7) and (8):

$$SF_0(\%) = \frac{\varepsilon_{0,un}}{\varepsilon_{def}} . 100 \quad (7)$$

$$SF_{600}(\%) = \frac{\varepsilon_{600un}}{\varepsilon_{def}} . 100 \quad (8)$$

where ε_{def} is the applied deformation and ε_{0un} and ε_{600un} represent the deformation of the specimen at load removal and 600 s after load removal, respectively. The subscript 0 and 600 refer to the time in seconds, after the beginning of step IX, at which strain fixity was evaluated.

Strain recovery at the end of step XII, SF_{3600}, was defined according to Equation (9):

$$SR_{3600}(\%) = \frac{\varepsilon_{def} - \varepsilon_{3600res}}{\varepsilon_{def}} . 100 \quad (9)$$

where $\varepsilon_{3600res}$ is the residue deformation at the end of the isothermal step. Also in this case, the subscript 3600 refers to the time in seconds, after the beginning of step XII, at which strain recovery was evaluated.

3 | RESULTS AND DISCUSSION

The effect of the production process and paraffin concentration on the morphological characteristics of the

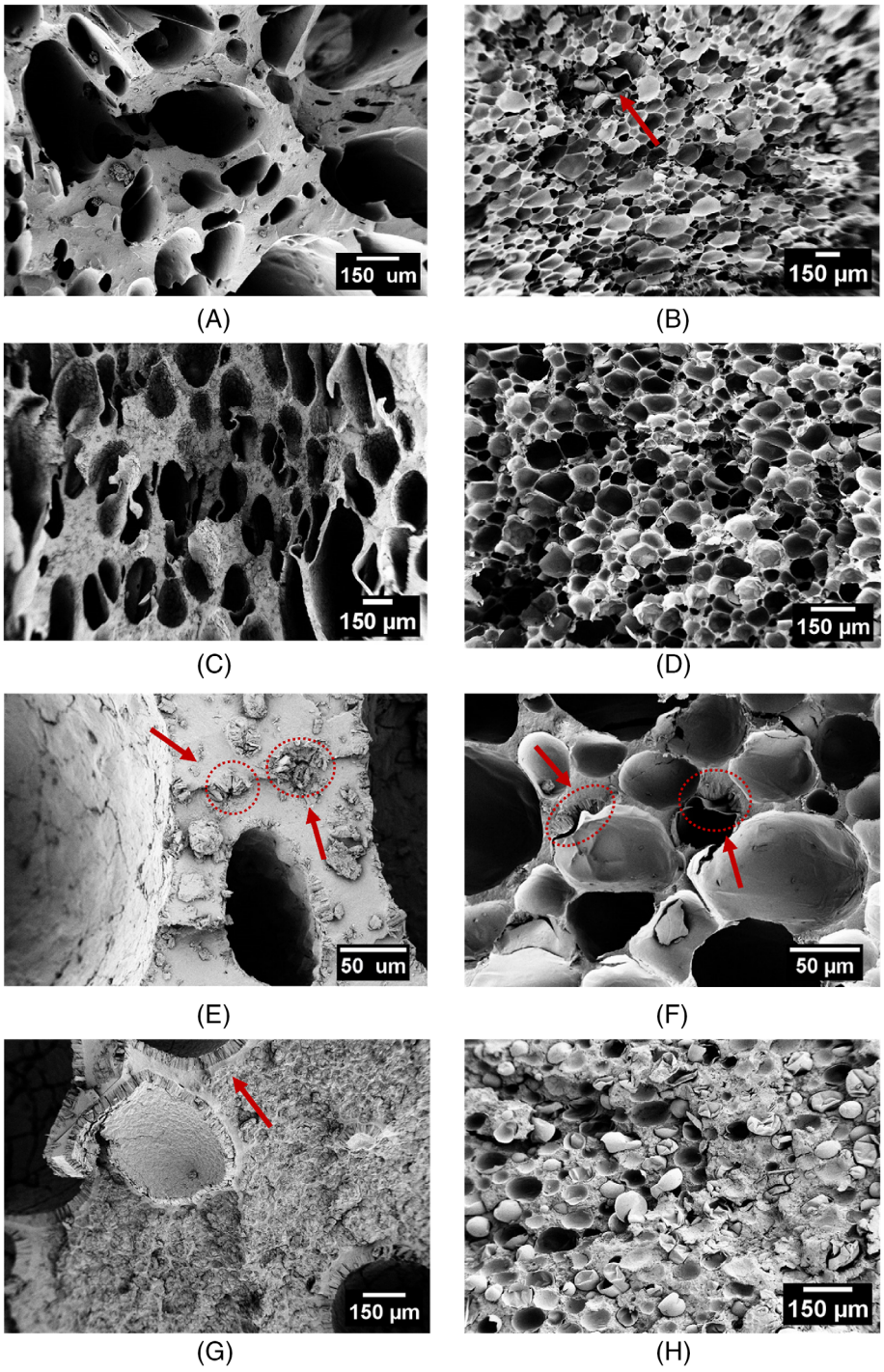

FIGURE 4 Scanning electron microscope (SEM) micrographs at different magnifications of the cryofracture surface of the prepared foams (A) EPDM_H; (B) EPDM_MP; (C–E) EPDM_H_P20; (D–F) EPDM_MP_P20; (G) EPDM_H_P60; and (H) EPDM_MP_P60. The red arrow indicates in Figure 4B the microcapsules containing the physical blowing agent, in Figures 4E, F the accumulation of paraffin in the EPDM matrix, and finally, in Figure 4G the presence of peculiar morphology.

produced foams was examined using SEM. The morphology of the foams has been already presented and discussed in our previous work on these systems.[34] In this study, some considerations of new morphological aspects were addressed. Figure 4A–F shows micrographs at various magnifications of the cryofracture surfaces of neat and paraffin-filled foams, while Table 3 gives information on the average pore diameter of the samples.

As can be observed in Figures 4A, B, the production process strongly affects the morphology of the foams.

TABLE 3 Dimension of the pores of the produced foams.

Sample	Diameter of the pores (µm)
EPDM_H	271 ± 150
EPDM_H_P20	254 ± 95
EPDM_H_P60	366 ± 306
EPDM_MP	110 ± 46
EPDM_MP_P20	82 ± 39
EPDM_MP_P60	64 ± 22

When H is used as a foaming agent, both open and closed porosity, which have a wide pore dimension distribution, (271 ± 150 μm), form. On the contrary, in the case of EPDM_MP, the foam has closed porosity, with a homogeneous shape and quite a uniform cell size (110 ± 46 μm). Red arrows in Figure 4B show that some of the fractured cells still have microcapsules (of the foaming agent MP) inside them. The cell geometry is another characteristic that distinguishes the two types of foams: cells are both spherical and elliptical in EPDM_H, mostly spherical in EPDM_MP.

The foams produced with 20 wt% of paraffin are shown in micrographs in Figure 4C–F. Compared to the corresponding neat sample, the pore size distribution of EPDM_H_P20 foam (Figure 4C) is more homogeneous, which is likely connected to the presence of PCM, which acts as a plasticizer and facilitates the foaming process. On the other hand, paraffin appears to make rubber expansion in the EPDM_MP_P20 sample more challenging since the cells are not only smaller (see Table 3), but also less spherical and homogeneous in shape than those in the neat foam. This different behavior may be attributed to the way paraffin distributes inside the EPDM matrix. As shown in Figure 4E, F, the PCM tends to form spherical drops in EPDM_H_P20, while in the case of EPDM_MP_P20 PCM tends to distribute around the microcapsules containing iso-pentane. The lower surface tension of microcapsules compared to the EPDM matrix may explain the paraffin accumulation on the microcapsules' surface. If the microcapsule shell material has a surface tension similar to or lower than that of paraffin, paraffin will tend to accumulate on the surface of the microcapsules. This low surface tension would also explain the spherical shape assumed by the PCM in EPDM_H_P20, as paraffin tries to reduce the contact surface with the EPDM matrix. However, further investigations should be carried out to confirm this hypothesis.

Finally, Figure 4G, H shows micrographs of EPDM foams containing 60 wt% of paraffin. As evidenced by the arrow in Figure 4G, EPDM_H_P60 presents a peculiar morphology. Between two layers of paraffin, one of which is dispersed lamellar over the surface of the pores and the other of which forms the walls of the foam, is a compact layer of EPDM. This is just another instance of the two phases' immiscibility. With increasing paraffin content, the average diameter of all foams produced with MP as a foaming agent gradually decreases. As was previously explained, paraffin probably tends to make rubber expansion more difficult in these kinds of foams.

Density measurements were performed, together with estimations of the proportions of closed and total porosity, in order to correlate the morphology of EPDM and EPDM/paraffin foams with their porosity values. Figure 5A, B presents the key findings. As well as SEM analysis, also the porosity evaluation has been discussed in our previous work. However, since the morphology of the foams could be one of the parameters affecting the shape memory properties of the samples, it was found fundamental to recall the main findings.

Density measurements confirm the conclusions reported for SEM observations. The results show that MP-foamed rubbers are mainly characterized by closed-cell porosity, while the H-foamed samples present a mixed open-cell/closed-cell morphology. Furthermore, foams produced with MP show the highest values of total porosity and, consequently, the lowest density. The morphological differences found among the produced foams are correlated to the distinct working principle of the two foaming agents. In the case of MP, the vaporization of the iso-pentane at 115°C is responsible for the microcapsules expansion and, as a result, for the generation of closed cells. Instead, in foams produced with the foaming agent H, the expansion is attributable to the evolution of CO_2 and vapor deriving from the thermal decomposition of sodium, potassium, and calcium bicarbonates dispersed in the EPDM matrix, which results in the development of both open and closed cells.

By adding more paraffin, the total porosity of all the produced foams decreases. The samples' capacity to expand is likely hampered by the PCM, which inhibits the release of gases (in the case of the H foaming agent) and reduces microcapsule expansion (in the case of the MP foaming agent). As can be observed in Figure 5A, B, the reduction of P_{tot} is more significant in MP-foamed samples.

The produced foams were characterized through dynamic mechanical analysis to identify the best conditions for shape memory tests. More specifically, DMA analysis was performed to identify the temperature region in which the melting of paraffin occurs and to select the temperature range in which to study the shape memory behavior of the EPDM/paraffin foams. Storage modulus, loss modulus, and loss factor as a function of temperature are presented in Figure 6A–F while the results of the DMA tests on the prepared foams are listed in Table 4.

The first-order transition, due to the melting of paraffin, occurs over a wide temperature range between 40 and 90°C for all EPDM/paraffin foams. This transition is clearly visible by looking at the loss factor plots (Figure 6C–F). The storage modulus decreases markedly in the temperature range 65–90°C and this effect is increasingly evident with increasing paraffin concentration. Above 90°C, a well-defined plateau is present, with values very close to the respective neat EPDM foams. The intensity of the loss factor and loss modulus progressively

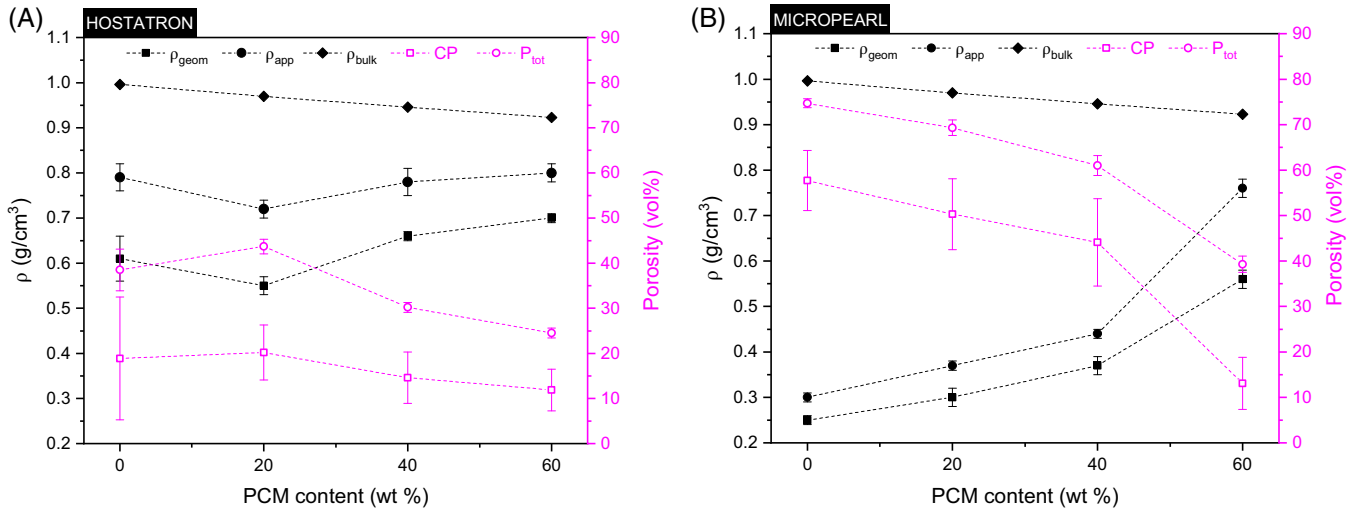

FIGURE 5 Density (ρ_{geom}, ρ_{app}, ρ_{bulk}) and close (CP) and total porosity (P_{tot}) of (A) foams produced with H and (B) foams produced with MP.

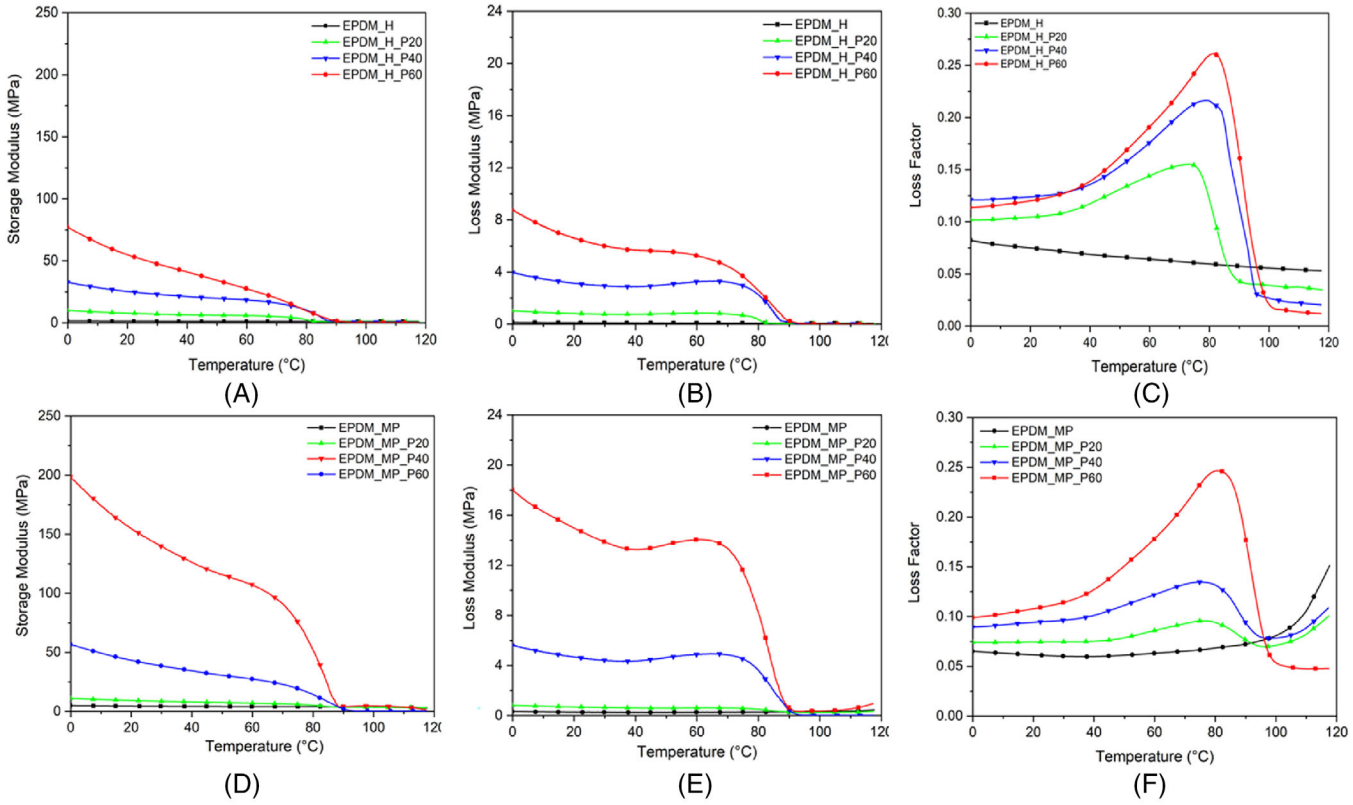

FIGURE 6 Storage modulus, loss modulus, and loss factor of neat and paraffin-filled foams produced with (A–C) H and (D–F) MP foaming agents.

increases with the PCM content, while the corresponding peaks remain in all the cases close to a temperature of 70–80 and 80°C, respectively.

Since at 90 and 25°C the melting and solidification of paraffin are completed, respectively, these temperatures were selected for exploring the shape memory behavior of the foams. The temperature at which the foams were deformed to the temporary shape was specifically chosen to be 90°C. On the other hand, 25°C was chosen as the temperature at which the deformed samples were cooled down, under a constant strain, to fix the temporary shape. The storage moduli of the prepared foams at

TABLE 4 Results of DMA tests on the prepared foams.

Sample	Storage modulus (MPa) at 25°C	Storage modulus (MPa) at 90°C
EPDM_H	1.40	1.28
EPDM_H_P20	7.43	1.04
EPDM_H_P40	24.13	0.60
EPDM_H_P60	51.04	1.63
EPDM_MP	4.43	4.01
EPDM_MP_P20	9.02	3.71
EPDM_MP_P40	40.81	2.16
EPDM_MP_P60	146.99	4.33

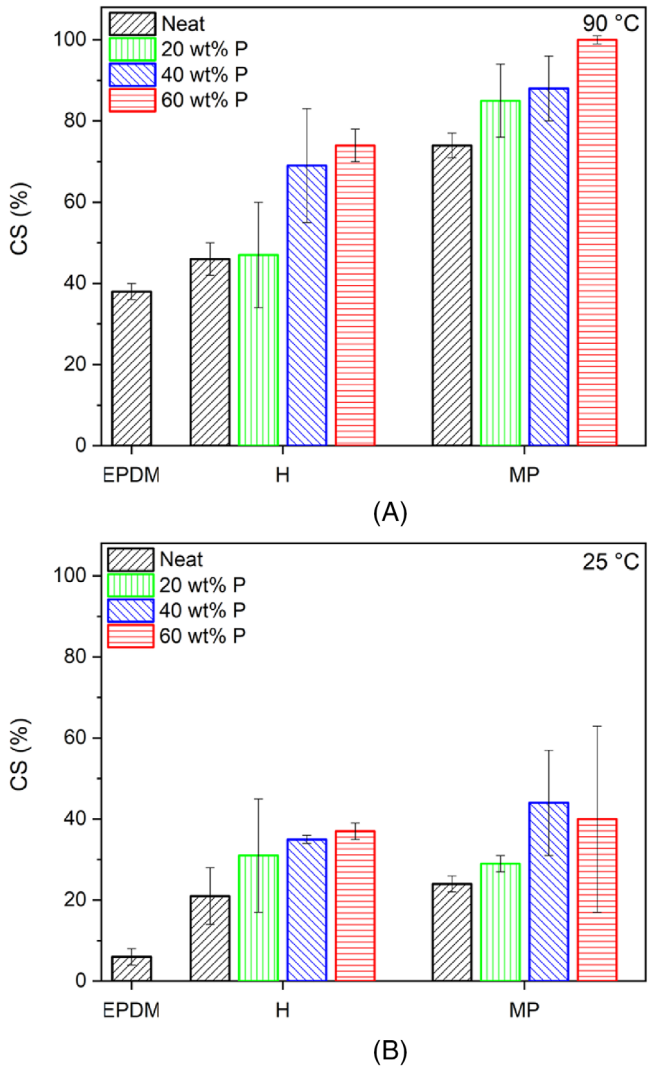

FIGURE 7 Results of the compression set at (A) 25°C and (B) 90°C on the prepared foams.

25 and 90°C are reported in Table 4. By passing from 25 to 90°C, the storage modulus drops by two orders of magnitude for EPDM_H_P60 and EPDM_MP_P60 and by one order of magnitude for all other samples. A sharp drop and a reduction at least of 2 orders of magnitude in storage modulus are required to achieve an excellent shape memory effect.[40] Consequently, optimum shape memory performance can be expected in EPDM_H_P60 and EPDM_MP_P60 foams.

The results of the compression set (CS) are reported in Figure 7A, B, which shows the permanent deformation values obtained from the CS tests at 25 and 90°C.

Focusing at first on CS values obtained at 25°C, it can be observed that EPDM_MP and EPDM_H foams show lower recovery properties than bulk EPDM rubber (6%). Indeed, they present quite high CS values (24% and 21%, respectively), probably attributable to the collapse of close cells under compression. In all the prepared foams, the addition of paraffin leads to an increase in permanent deformation and this effect is generally more evident with an increase in the paraffin amount. Comparing the results at 25°C with those obtained at 90°C, the strong influence of temperature on both neat foams and paraffin-filled samples can be noticed. In particular, a significant increase in permanent deformation has been registered moving to 90°C. This result, in samples containing the PCM, could be probably related to paraffin solidification occurring during the recovery time. The progressive solidification could have made the recovery to original conditions more difficult, as suggested by the increasing CS values with increasing paraffin content. Among the produced paraffin-filled samples, foams produced with MP are almost unable to recover the deformation. The sample EPDM_MP_P60 deserves special consideration for which a compression set value equal to 100 is obtained.

The shape memory response of the produced EPDM/paraffin foams was investigated following a two-step analysis. Firstly, a preliminary study of the shape memory behavior of the samples was carried out to verify the effective role of paraffin in improving the shape memory performance of neat EPDM foams. After that, a quantitative analysis of the shape memory behavior was performed. Focusing at first on the results obtained in the preliminary analysis, the digital images representing the recovery process at 90°C of the produced foams are reported in Figure 8A, B while the strain fixity (SF_0) and strain recovery (SR) values determined at different times (0, 100, 200, 500, 1100, and 1800 s) are presented in Figure 9A, B–D, respectively.

From digital images taken at 0 s, it is evident that the neat foams are not able to fix the temporary shape. This is confirmed by looking at the SF_0 values reported in Figure 8A. In particular, the EPDM_H sample shows a strain fixity value of 16.8%, while the EPDM_MP of 31.0%.

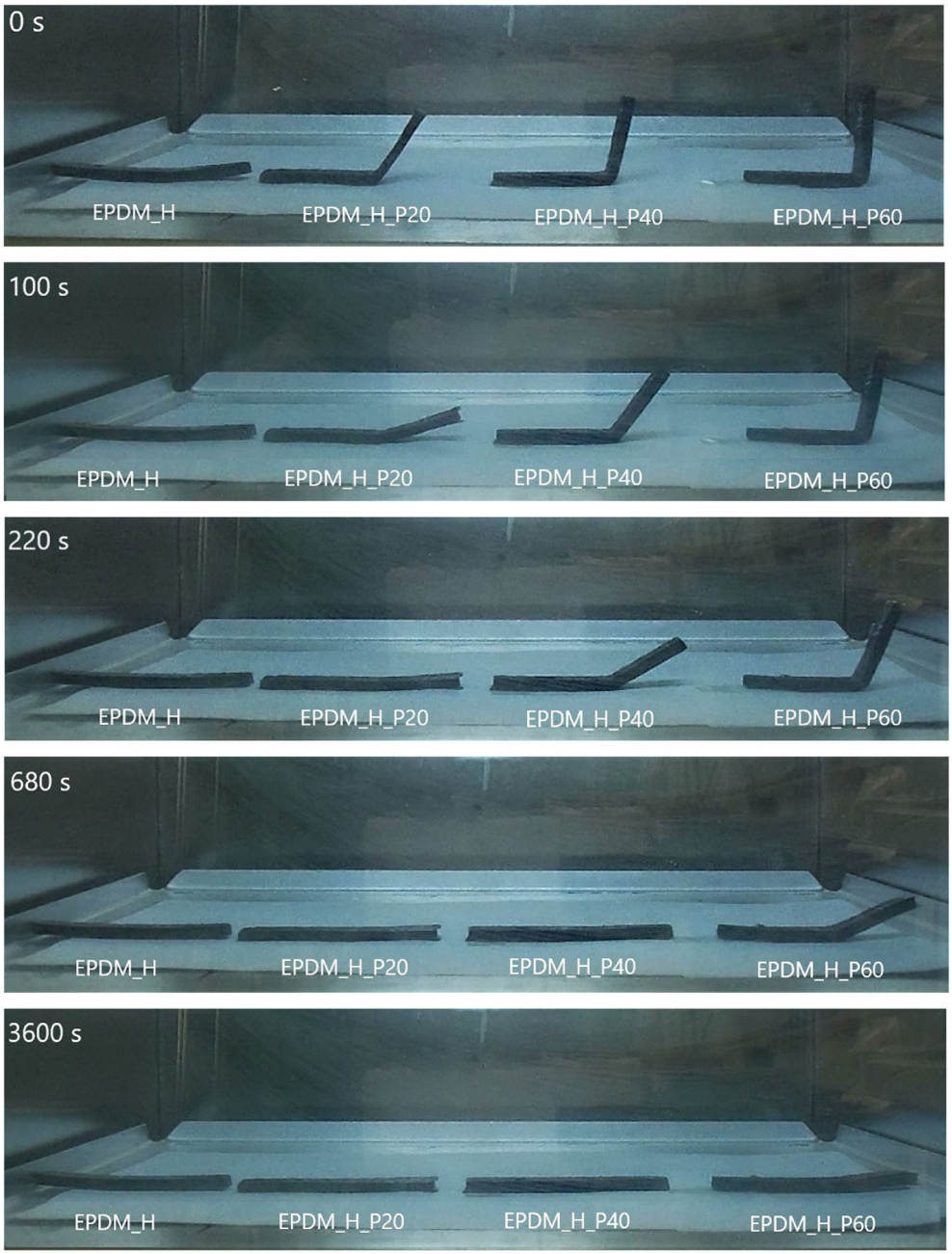

FIGURE 8 Digital images representing the recovery process of neat and paraffin-filled foams produced with (A) H and (B) MP foaming agents.

Focusing on EPDM/paraffin foams, for all samples the strain fixity values progressively increase with PCM content; clear evidence of the crucial role played by paraffin in providing excellent shape fixability for EPDM/paraffin foams. Even an amount of PCM as small as 20% can raise the strain fixity parameter to 62% and 65% in samples produced with H and MP, respectively. A complete fixing of the permanent shape (and so an $SF_0 = 100\%$) has been found only in the EPDM_MP_P60 sample, as expected from the results of the CS tests. To give a more quantitative relationship between the influence of paraffin content and the type of foams on the recovery behavior, Figure 9B, C show the graphical representation of the strain recovery (SR) values evaluated at 0, 100, 200, 500, 1100, and 1800 s. As shown in Figure 9, the higher the paraffin content, the slowest the recovery process of the foams. At a given PCM content, the expanded rubbers exhibit similar recovery behavior, but

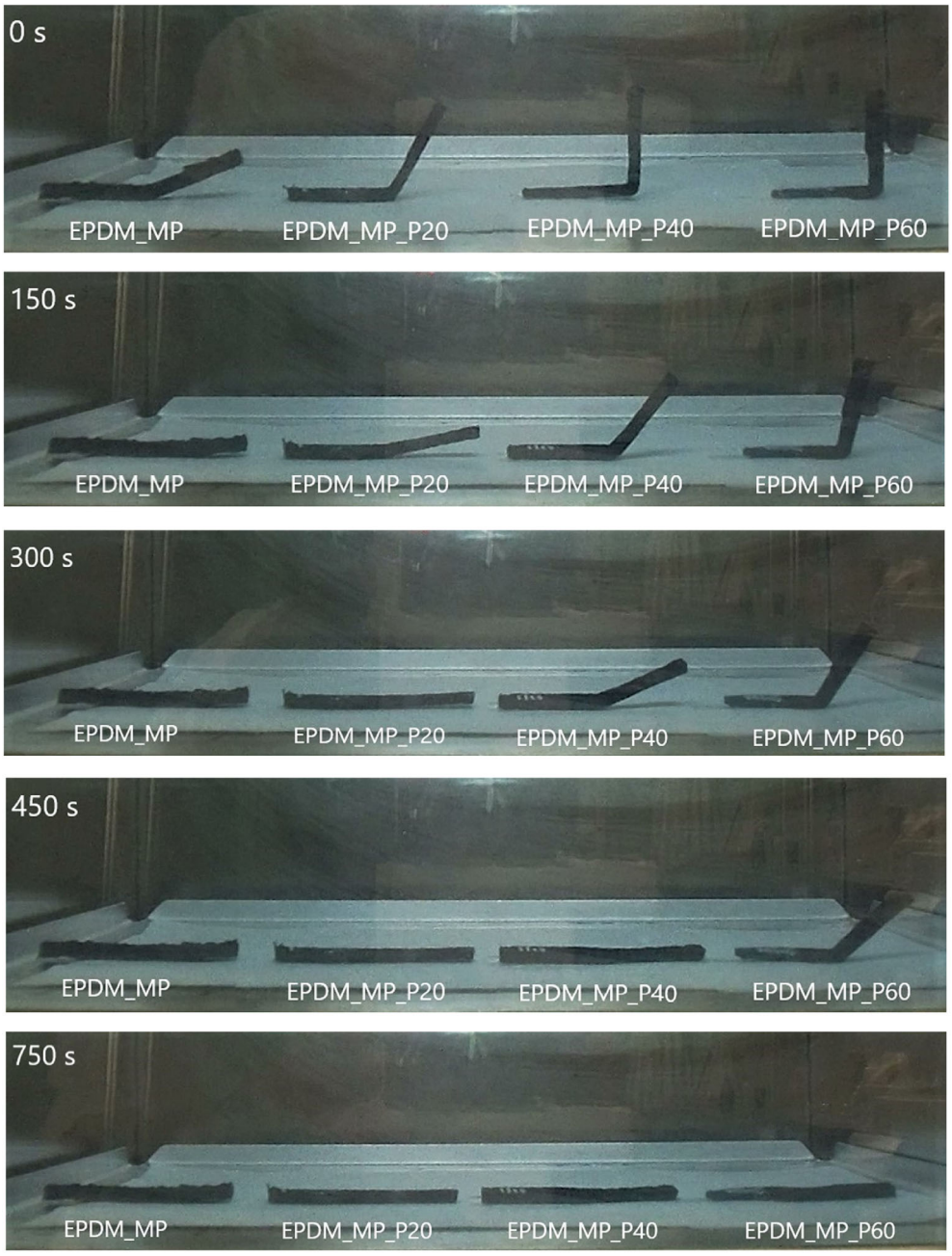

FIGURE 8 (Continued)

slightly higher recovery kinetics is detectable in the case of MP-foamed samples. Finally, EPDM_H_P60 is the only sample that at 1800 s (30 min) has not yet returned to the permanent shape. As shown in Figure 8A, more time is required for this foam (about 1 h). In conclusion, the analysis has revealed the fundamental role of paraffin in improving the shape memory performance of neat foams. At room temperature, crystalline paraffin is responsible for fixing the bent temporary shape of the samples. Upon heating above the melting temperature of the PCM, paraffin melts and promotes the return of the foams to the original condition. The results obtained have brought to light that also foams morphology and paraffin distribution probably play a role in dictating the shape memory performance of the samples. Indeed, the expanded rubbers produced with MP, which present mainly closed-cell porosity and in which the PCM accumulated preferentially onto the surface of the microcapsules, presented the best compromise between fixability and recovery ability. The positive results obtained have allowed studying more

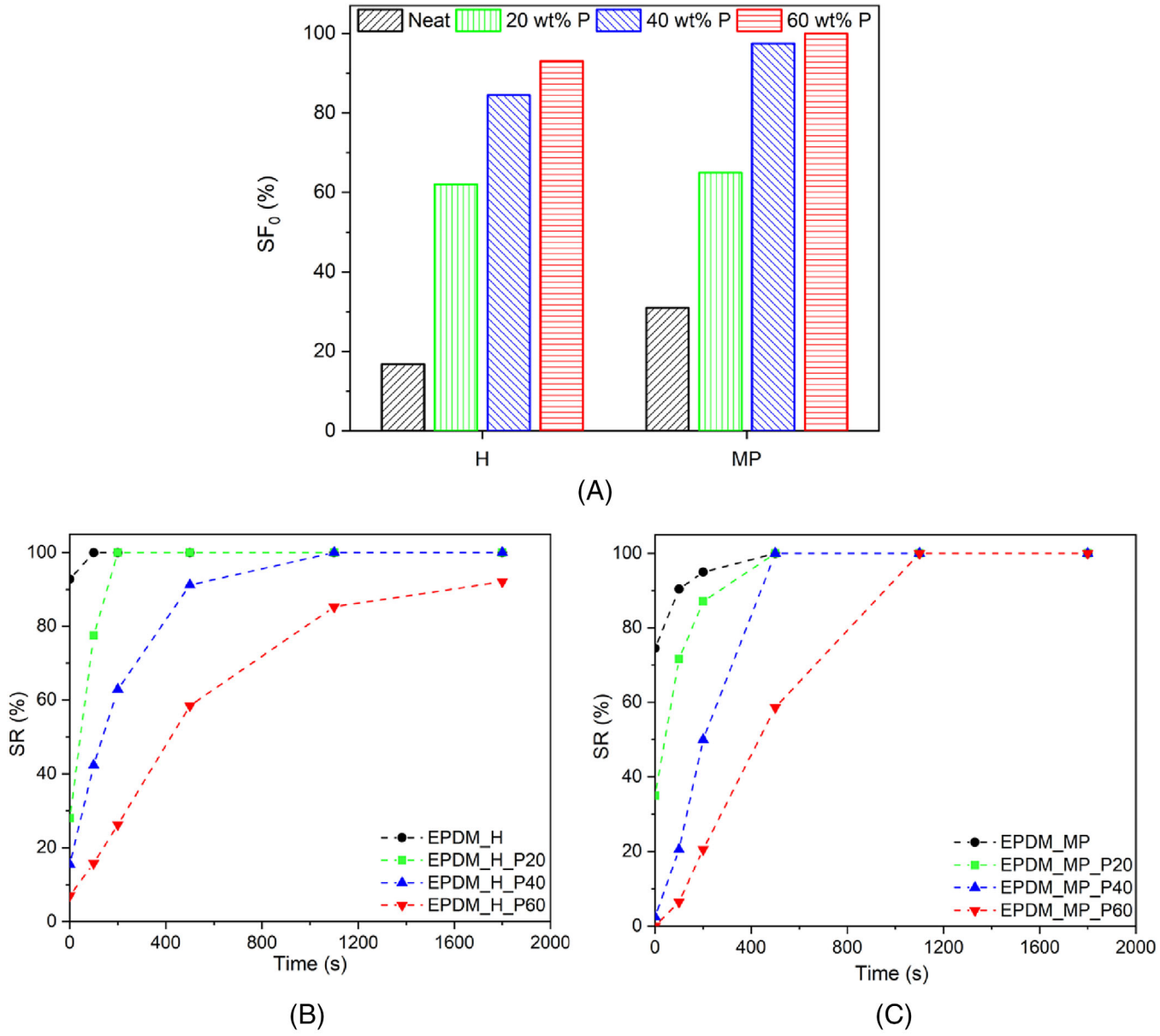

FIGURE 9 (A) Strain fixity (SF_0) and (B, C) strain recovery (SR) as a function of time for the recovery test at 90°C of foams produced with H and MP foaming agents.

accurately the shape memory behavior of the samples through DMA. The results of the DMA tests on the foams' shape memory behavior are reported in Figure 10A, B.

Looking at Figures 10A, B, conclusions formed in the preliminary analysis are generally confirmed here. EPDM_H foam shows poor capability in fixing the temporary shape, with an SF_0 value equal to 21.8%. On the other hand, the EPDM_MP sample presents much better shape-fixing properties, with a strain fixity value at load removal corresponding to 71.3%. While EPDM_H shows quite similar values of SF_0 to those determined in the preliminary analysis, a significant difference is found here for EPDM_MP foam, namely the strain fixity parameter in the preliminary analysis is significantly lower than that measured here. This experimental evidence could be correlated to the compression set values reported in Figure 7: EPDM_MP sample, both at 25 and 90°C, presents the highest permanent deformation that could explain greater SF_0 values. However, also the distinct way the specimens were deformed in the two analyses may have affected the strain fixity parameters of these samples. Further investigations should be carried out to confirm this last hypothesis.

The addition of paraffin increases SF_0 values in the foams and, by increasing the PCM loading, the strain

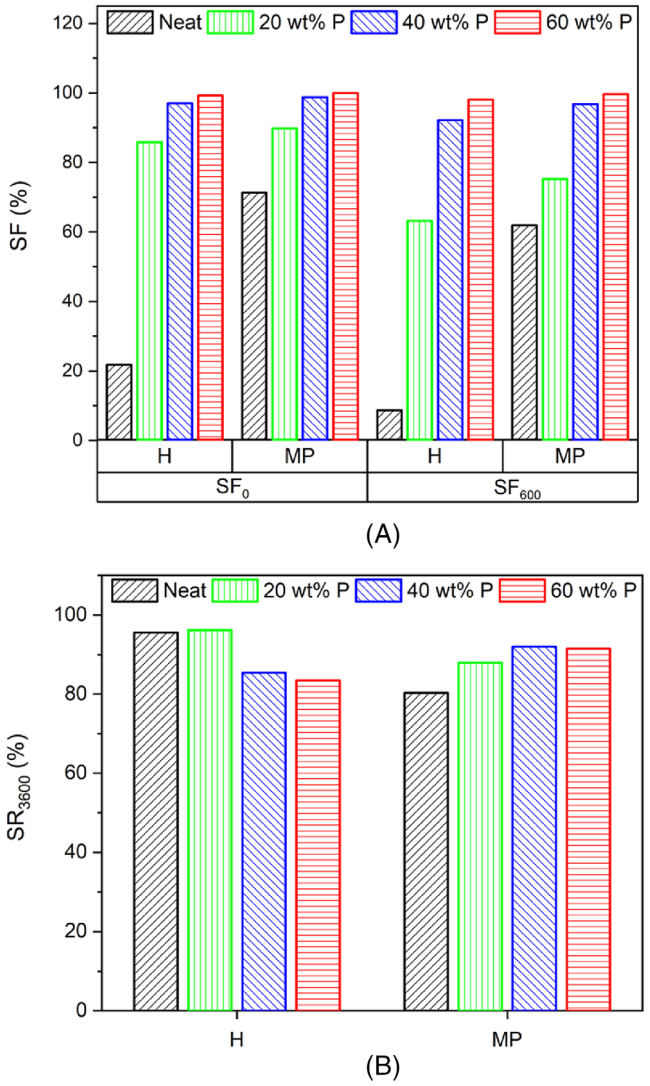

FIGURE 10 (A) Strain fixity (SF_0 and SF_{600}) and (B) strain recovery (SR_{3600}) of the prepared neat and paraffin-filled foams.

fixity parameter increases as well. The strain fixity parameters derived from DMA tests are higher than those obtained from the preliminary analysis (see Figure 9A). For example, values greater than 85% have been determined with only 20 wt% of PCM, compared to only 62% from the bend-recovery tests. As was previously hypothesized, this behavior is probably associated with the distinct way the foams were deformed. The strain fixity parameter 10 min after load removal (SF_{600}) shows that part of the deformation is recovered at 25°C since SF_{600} results are lower than SF_0 in all the studied samples. However, the duration of the strain fixability improves with increasing PCM content. For example, in EPDM_MP_P60 and EPDM_H_P60 samples SF_{600} and SF_0 differ by 1.2% and 0.3%, respectively. This result underlines that the amount of paraffin plays an important role in maintaining over time the temporary shape of the foams.

Finally, the recovery behavior of H- and MP-foamed rubbers shows different trends. For MP-foamed rubbers, SR_{3600} clearly increases with the PCM content; for H-foamed samples, a slight reduction in this parameter is noted at higher paraffin loadings. As noted in the preliminary analysis, foams produced with H as a foaming agent probably require more time to return to the original shape with PCM. However, all paraffin-filled foams show a percentage of shape recovery higher than 84%, meaning that the main part of deformation is recovered in 1 h at 90°C. EPDM_H_P20 is characterized by the highest SF_{3600} value (96.2%) followed by EPDM_MP_P40 (92%).

4 | CONCLUSIONS

This work demonstrated the efficacy of a PCM such as paraffin in conferring shape memory properties to EPDM/paraffin foams. Samples filled with different amounts of paraffin were prepared by melt compounding and hot-pressing and characterized thermo-mechanically. The foaming agent Micropearl F82® (MP) produced a closed-cell morphology, while Hostatron P0168® (H) led to the formation of a mixed closed-cell/open-cell porosity, according to SEM micrographs and density measurements. By increasing the PCM content, the total porosity decreased in all EPDM/paraffin foams, probably due to the action of the PCM to hinder the expansion of the samples.

DMA analysis revealed that the melting of paraffin occurred over a wide temperature range between 40 and 90°C for all EPDM/paraffin foams. Since at 90 and 25°C the melting and solidification of the PCM are completed, respectively, these temperatures were selected for exploring the shape memory behavior of the samples. 90°C was chosen as the temperature at which the foams were deformed to the temporary shape while 25°C was chosen as the temperature to which the deformed samples were cooled, under constant strain, to fix the temporary shape.

From shape memory tests, the crucial role played by the PCM in providing excellent shape fixability for the expanded rubber was demonstrated. Even an amount of paraffin as small as 20 wt% resulted in strain fixity values higher than 60% for qualitative bend-recovery tests, and above 80% in the case of DMA shape memory quantitative tests. With increasing paraffin concentration, the shape fixability of the foams improved, but the recovery process became slower. Consequently, a compromise between a fast recovery and optimum shape fixability should be determined. Among the foams studied, the ones produced with MP seem to be the most promising,

since they presented both the highest strain fixity parameters and the fastest recovery process.

PCM played a key role in the multifunctionality of the produced EPDM/paraffin foams. At the same time, PCM provided good TES properties, as was reported in our previous work,[34] and optimum shape memory performance to the expanded rubbers. The shape variation and TES capabilities could make EPDM/paraffin foams potentially easier to be installed and interesting to be used for thermal management applications. Future research will aim to determine the duration of the strain fixability, that is, the time in which these EPDM/paraffin foams can be stored at room temperature while keeping the temporary shape.

DATA AVAILABILITY STATEMENT

The data that support the findings of this study are available from the corresponding author upon reasonable request.

ORCID

M. Bianchi https://orcid.org/0000-0002-2083-7524
G. Fredi https://orcid.org/0000-0001-9987-1786
F. Valentini https://orcid.org/0000-0001-9496-0501

REFERENCES

[1] J. Hu, Y. Zhu, H. Huang, J. Lu, *Prog. Polym. Sci.* **2012**, *37*, 1720.
[2] Y. Liu, H. Du, L. Liu, J. Leng, *Smart Mater. Struct.* **2014**, *23*, 23001.
[3] W. Small IV., P. Singhal, T. S. Wilson, D. J. Maitland, *J. Mater. Chem.* **2010**, *20*, 3356.
[4] C. M. Yakacki, R. Shandas, C. Lanning, B. Rech, A. Eckstein, K. Gall, *Biomaterials* **2007**, *28*, 2255.
[5] C. Liu, H. Qin, P. T. Mather, *J. Mater. Chem.* **2007**, *17*, 1543.
[6] S. Pandini, F. Baldi, K. Paderni, M. Messori, M. Toselli, F. Pilati, A. Gianoncelli, M. Brisotto, E. Bontempi, T. Riccò, *Polymer* **2013**, *54*, 4253.
[7] H. Kalita, *Shape Memory Polymers: Theory and Application*, 1st ed., De Gruyter, Boston **2018**.
[8] M. Behl, A. Lendlein, *Mater. Today* **2007**, *10*, 20.
[9] J. Parameswaranpillai, *Shape Memory Polymers, Blends and Composites*, 1st ed., Springer, New York **2020**.
[10] H. Zhang, H. Wang, W. Zhong, Q. Du, *Polymer* **2009**, *50*, 1596.
[11] A. Reghunadhan, K. P. Jibin, A. V. Kaliyathan, P. Velayudhan, M. Strankowski, S. Thomas, *Materials* **2021**, *14*, 14237216.
[12] Z. Ding. PhD thesis, Nanyang Technological University, Singapore. **2012**.
[13] L. Sun, W. M. Huang, Z. Ding, Y. Zhao, C. C. Wang, H. Purnawali, et al., *Mater. Des.* **2012**, *33*, 577.
[14] S. M. Lai, G. L. Guo, *Polym. Test.* **2019**, *77*, 105892.
[15] D. Fernandes, F. Pitié, G. Cáceres, J. Baeyens, *Energy* **2012**, *39*, 246.
[16] M. Karkri, M. Lachheb, F. Albouchi, S. B. Nasrallah, I. Krupa, *Energ. Buildings* **2015**, *88*, 183.
[17] L. Xing, L. Hongyan, W. Shujun, Z. Lu, C. Hua, *Sol. Energy* **2006**, *80*, 1561.
[18] S. D. Sharma, K. Sagara, *Int. J. Green Energy* **2005**, *2*, 1.
[19] Y. Shi, B. Zhou, *Energ. Buildings* **2019**, *183*, 650.
[20] P. Sánchez, M. V. Sánchez-Fernandez, A. Romero, J. F. Rodríguez, L. Sánchez-Silva, *Thermochim. Acta* **2010**, *498*, 16.
[21] M. Jiang, X. Song, G. Ye, J. Xu, *Compos. Sci. Technol.* **2008**, *68*, 2231.
[22] J. F. Su, X. Y. Wang, S. B. Wang, Y. H. Zhao, Z. Huang, *Energy Convers. Manag.* **2012**, *55*, 101.
[23] H. Deng, W. Yang, T. Cai, F. He, Y. Li, K. Zhang, R. He, *Int. J. Energy Res.* **2021**, *45*, 18033.
[24] S. Kahwaji, M. B. Johnson, A. C. Kheirabadi, D. Groulx, M. A. White, *Energy* **2018**, *162*, 1169.
[25] D. Rigotti, A. Dorigato, A. Pegoretti, *Mater. Today Commun.* **2018**, *15*, 228.
[26] G. Fredi, A. Dorigato, L. Fambri, A. Pegoretti, *Multifunct. Mater.* **2020**, *3*, 2001.
[27] G. Fredi, A. Dorigato, L. Fambri, A. Pegoretti, *Compos. Sci. Technol.* **2018**, *158*, 101.
[28] F. Valentini, A. Dorigato, L. Fambri, A. Pegoretti, *Rubber Chem. Technol.* **2021**, *94*, 432.
[29] F. Valentini, L. Fambri, A. Dorigato, A. Pegoretti, *Front. Mater.* **2021**, *8*, 660656.
[30] F. Valentini, L. Fambri, A. Dorigato, A. Pegoretti, *Front. Mater.* **2021**, *8*, 101.
[31] Q. Zhang, J. Feng, *Sol. Energy Mater. Sol. Cells* **2013**, *117*, 259.
[32] H. Y. Wu, S. T. Li, Y. W. Shao, X. Z. Jin, X. D. Qi, J. H. Yang, Z. W. Zhou, Y. Wang, *Chem. Eng. J.* **2020**, *379*, 122373.
[33] J. H. Jing, H. Y. Wu, Y. W. Shao, X. D. Qi, J. H. Yang, Y. Wang, *ACS Appl. Mater. Interfaces* **2019**, *11*, 19252.
[34] M. Bianchi, F. Valentini, G. Fredi, A. Dorigato, A. Pegoretti, *Polymer* **2022**, *14*, 4058.
[35] E. Rostami-Tapeh-esmaeil, A. Vahidifar, E. Esmizadeh, D. Rodrigue, *Polymer* **2021**, *13*, 1565.
[36] A. W. Birley, in *Handbook of Plastic and Elastomers*, 4th ed. (Ed: C. A. Harper), M-H editor, New York **1975**.
[37] W. D. Callister, *Materials Science and Engineering*, 7th ed., John Wiley & Sons, New York **2007**.
[38] D. Eaves, *Handbook of polymer foams*, 1st ed., Rapra Technology Ltd., Shrewsbury **2004**.
[39] V. Luca, A. L. M. Miguel, *High-Performance Elastomeric Materials Reinforced by Nano-Carbons: Multifunctional Properties and Industrial Applications*, 1st ed., Elsevier, Amsterdam **2020**.
[40] Y. Li, W. Pan, F. Zhang, J. Leng, *J. Intell. Mater. Syst. Struct.* **2021**, *33*, 1762.

How to cite this article: M. Bianchi, G. Fredi, F. Valentini, A. Dorigato, A. Pegoretti, *Polym. Eng. Sci.* **2023**, *63*(5), 1633. https://doi.org/10.1002/pen.26312